Electrical neuromodulation biases brightness perception of flickering light

Neural codes of brightness perception

Marina Fiene[1*], Jan-Ole Radecke[1], Jonas Misselhorn[1], Malte Sengelmann[1], Christoph S. Herrmann[2,3], Till R. Schneider[1], Bettina C. Schwab[1&], Andreas K. Engel[1&]

[1] Department of Neurophysiology and Pathophysiology, University Medical Center Hamburg-Eppendorf, Hamburg, Germany

[2] Experimental Psychology Lab, Department of Psychology, Cluster of Excellence "Hearing4all", European Medical School, Carl von Ossietzky University, Oldenburg, Oldenburg, Germany

[3] Research Center Neurosensory Science, Carl von Ossietzky University Oldenburg, Oldenburg, Germany

[&] shared last authorship

* Corresponding author

Marina Fiene

E-mail: m.fiene@uke.de

Abstract

Human brightness estimation often pronouncedly dissociates from objective viewing conditions. Yet, the physiological substrate underlying subjective perception is still poorly understood. Rather than physical illumination, the subjective experience of brightness has been shown to correlate with temporal dynamics in the amplitude of cortical neural responses. Here, we aimed to experimentally manipulate visual flicker-evoked steady-state responses and related perception via concurrent modulation of cortical excitability by transcranial alternating current stimulation. Participants performed a brightness discrimination task of two visual flicker stimuli, one of which was targeted by same-frequency electrical stimulation at varying phase shifts. Transcranial electrical stimulation was applied with an occipital and a periorbital active control montage, based on finite-element method simulations of electric fields. Experimental results reveal that flicker brightness perception is modulated dependent on the phase shift between sensory and electrical stimulation, solely under stable flicker entrainment and exclusively under occipital electrical stimulation. The degree of induced brightness modulation was positively correlated with the strength of neuronal phase locking to the flicker, recorded prior to electrical stimulation. This finding was corroborated by a neural network model, demonstrating a comparable dependency between flicker-evoked phase synchronization and amplitude modulations of entrained neural rhythms by phase shifted visual and electric inputs. Our data suggest a causal role of the amplitude of neural activity in visual cortex for brightness perception in humans. This finding provides an important step towards understanding the basis of visual perception and further confirms electrical stimulation as a tool for advancing controlled modulations of neural excitability and related behavior.

Introduction

The estimation of brightness is a major task of the human visual system, yet, factors that determine the subjective experience of brightness and its physiological substrate are poorly understood. Depending on constituents of the visual scene, feedforward projections along the visual pathway are subject to complex neural computations that shape perception in addition to the physical level of illumination. A popular approach to examine the underlying mechanisms of brightness perception builds on frequency tagging of neuronal responses by sinusoidally modulated luminance stimuli that evoke continuous oscillatory signals in the visual cortex with highly predictable time course [1]. For instance, in response to flickering visual stimulation within or in regions outside the cells' receptive field, single-cell firing patterns were shown to reflect actual as well as illusory brightness percepts [2–5]. These entrained neuronal responses, correlated with the subjective experience of brightness, were found in primary visual cortex but not earlier in the visual pathway. Noninvasive neural population level recordings in humans of flicker entrained activity, i.e., visually evoked steady-state responses (SSRs), converge with these findings. The increase in physical luminance contrast of flickering stimuli has been shown to correlate with the amplitude of SSRs [6–9]. Further, the amplitude of cortical responses evoked by brightness induction stimuli was related to the strength of illusory brightness percepts as early as in primary visual cortex, as recorded by functional imaging or electroencephalography (EEG) [10–13]. Thus, the amplitude of rhythmic brain activity at first stages of cortical processing is assumed to not merely code physical stimulation properties but rather the subjective quality of perception.

Despite converging evidence about the role of the oscillatory amplitude in visual cortex for brightness perception, available data does not readily establish its functional relevance. A popular approach to test the causal relation between oscillatory neuronal activity and perception is based on non-invasive neuromodulation by externally applied electric fields [14,15].

Specifically, transcranial alternating current stimulation (tACS) is used with the aim to entrain neural activity by phase-specific excitability modulation in targeted brain regions. Invasive recordings in monkeys yielded key evidence that spike timing follows the phase of the applied electric current [16–18]. Only recently, we have shown that pairing tACS with same-frequency flicker results in systematic enhancement and suppression of flicker-evoked SSR amplitudes dependent on the phase shift between visual and electrical stimulation [19]. This finding corroborated the capability of tACS to shape neural responsiveness to natural visual inputs in humans [20,21]. Yet, crucially, whether this tACS-induced modulation of neural activity to flickering light also affects the subjective experience of flicker brightness has not been established. Evidence for behavioral deterioration or improvement by interfering with flicker-evoked neuronal responses would provide a strong claim about the functional relevance of the underlying brain rhythm.

Here, we asked whether biasing cortical processing of rhythmic visual stimulation by tACS under constant luminance conditions translates into perceptual changes. By using oscillatory entrainment via tACS, we aimed to modulate the amplitude of flicker-evoked responses by concurrent electrically-induced neuronal excitability modulation of the visual cortex. Participants performed a two-flicker brightness discrimination task, while tACS was simultaneously applied at one of the two flicker frequencies with systematic phase shift. We hypothesized that neural activity in the visual cortex, modulated by the phase shift between visually and electrically driven neuromodulation, causally influences perceptual changes of flicker brightness. Using EEG recordings prior to electrical stimulation, we find that tACS modulates the subjective experience of brightness in participants with stable flicker phase entrainment. Complemented by simulations of a neural network model, our data support a causal role of rhythmic brain activity in visual cortex for brightness perception.

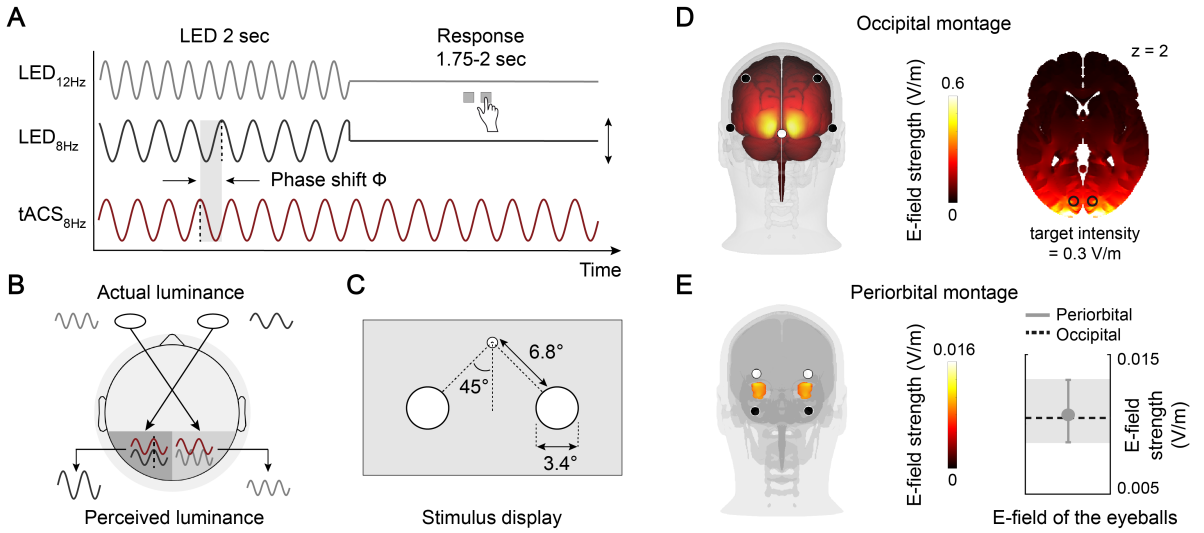

Fig 1. Experimental setup. (A) During continuous transcranial alternating current stimulation (tACS) at 8 Hz, participants were asked to judge per button press which of the two simultaneously presented flickers appeared brighter. Luminance of the LED_{8Hz} was varied while the LED_{12Hz} remained at constant luminance. The lag between LED_{8Hz} and tACS onset was systematically varied across six different phase shifts. (B) Schematic of the experimental hypothesis that phase-specific electrical stimulation of same-frequency flicker-evoked responses systematically modulates brightness perception. (C) The two flickers were presented simultaneously in the lower visual field while participants fixated the upper fixation dot. (D) During occipital tACS at 4 mA peak-to-peak, estimated maximum electric field strength was about 0.6 V/m, reaching 0.3 V/m in the target regions within the upper bank of the calcarine sulcus (MNI-coordinates: -10, -90, 2 and 10, -90, 2). (E) During the periorbital control condition, estimated electric field strength in the eyeballs for tACS intensities at 80% phosphene threshold was comparable to the field magnitude induced by occipital tACS due to current shunting across the scalp (periorbital: bootstrapped mean .01, 95%-CI).

Results

We recorded behavioral and EEG data from 38 participants in a highly controlled setup, that was complemented by electric field simulations and neural network modelling. Participants performed a two-flicker brightness discrimination task using flicker frequencies at 8 and 12 Hz, while multi-electrode tACS at 8 Hz was simultaneously applied at six different phase shifts (0°, 60°, 120°, 180°, 240°, 300°) relative to the 8 Hz flicker cycle (Fig 1A). Data were recorded during occipital and periorbital tACS on two separate days in counterbalanced order. The occipital tACS montage was chosen to maximize current density in the target region, i.e., the upper bank of the calcarine sulcus (Fig 1D) [22]. Stimulation intensity was set to 4 mA peak-to-peak. Estimated current densities by simulations based on finite-element head models (see

106 Materials and Methods) were in the region of electric field strengths shown to successfully
107 modulate neural activity in nonhuman primates and humans [18,23–25]. The periorbital control
108 montage was explicitly tailored for transretinal stimulation slightly below phosphene threshold
109 (Fig 1E). Thereby, we controlled for a potential confound of retinal co-stimulation under
110 occipital tACS due to current shunting across the scalp [26–28]. As the subjective perception
111 of flicker brightness is known to vary with the temporal modulation frequency [29,30], we first
112 determined the discrimination threshold of perceived brightness differences between the 8 Hz
113 tACS-targeted flicker (LED_{8Hz}) and the 12 Hz reference flicker (LED_{12Hz}) dependent on their
114 luminance ratio. Second, electrophysiological data without tACS were recorded to quantify
115 individual flicker entrainment strength on data segments free of electrical artifacts. Finally,
116 individually estimated psychometric functions were used for the main tACS experiment to
117 investigate tACS effects on flicker brightness discrimination around visual perception
118 threshold.

119

120 Individualization of physical flicker luminance intensity

121 In order to account for subjective differences in brightness perception between the two
122 flicker frequencies, we fit pychometric functions to the individual LED brightness
123 discrimination performance at varying LED luminance ratios (Fig 2A). The mean luminance
124 ratio between LED_{8Hz} and LED_{12Hz} at the 50 % discrimination threshold was .96 with a mean
125 standard error of .036. Thus, on average participants perceived the LED_{8Hz} as slightly brighter
126 compared to the LED_{12Hz}. The psychometric function was estimated on both testing sessions
127 with high retest-reliability, as shown by a significant correlation between the mean luminance
128 ratios within the 35 % and 65 % discrimination thresholds estimated per session ($r = .84$, $p <$
129 $.001$). Yet, to ensure identical visual stimulation for the two tACS conditions, participants were
130 presented with luminance ratios determined on the first day on both testing sessions. Median

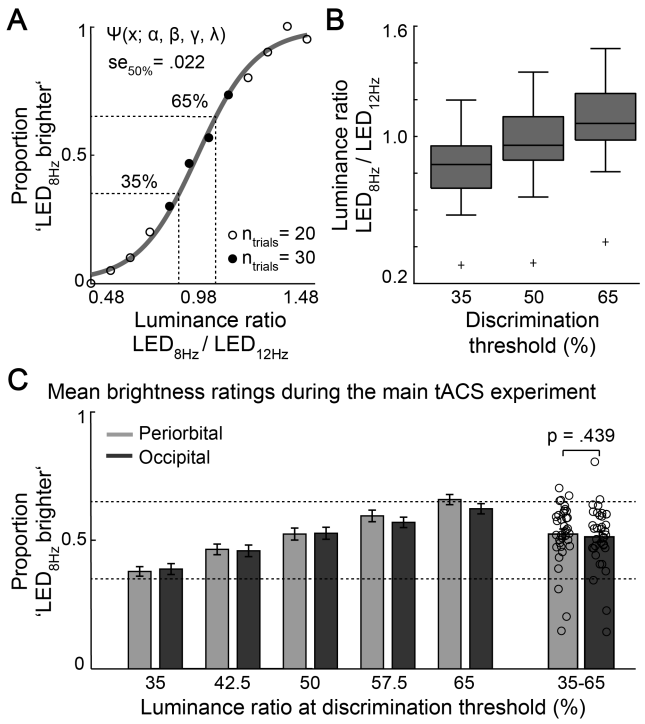

Fig 2. Individualization of physical luminance intensities around flicker brightness discrimination thresholds. (A) Psychometric function for one exemplary participant. Individual luminance ratios between LED_{8Hz} and LED_{12Hz} were determined between the 35 and 65 % brightness discrimination thresholds. (B) Distribution of the estimated luminance ratios between LED_{8Hz} and LED_{12Hz} across participants. (C) Bar diagram shows the proportion of trials on which the LED_{8Hz} was judged as brighter, averaged across flicker-tACS phase shifts during the main tACS experiment. As intended, depending on the luminance ratio between LED_{8Hz} and LED_{12Hz}, performance ranged between 35 and 65 % brighter judgements. There was no statistical difference between average judgements during the occipital and periorbital testing session.

peak luminance values for the LED_{8Hz} ranged between 78 and 102 cd/m^2 across brightness discrimination thresholds, while the LED_{12Hz} had a constant peak luminance of 95 cd/m^2.

For the main tACS experiment, trials were presented at five luminance ratios around discrimination threshold, at each of the six tACS-LED_{8Hz} phase shifts. To verify that participants accurately performed the brightness discrimination task, we averaged the proportion of brighter judgements of the LED_{8Hz} across tACS-LED_{8Hz} phase shift conditions, separately for each testing session. As shown in Fig 2C, the proportion of trials on which the LED_{8Hz} was rated as brighter ranged between 35 % and 65 % of judgements. Without taking flicker-tACS phase shifts into account, there was no significant difference between mean brighter ratings in the occipital and periorbital tACS condition across luminance ratios ($t(35) = -0.78$, $p = .439$, $d_z = -.13$).

Interindividual differences in phase stability of visually evoked responses

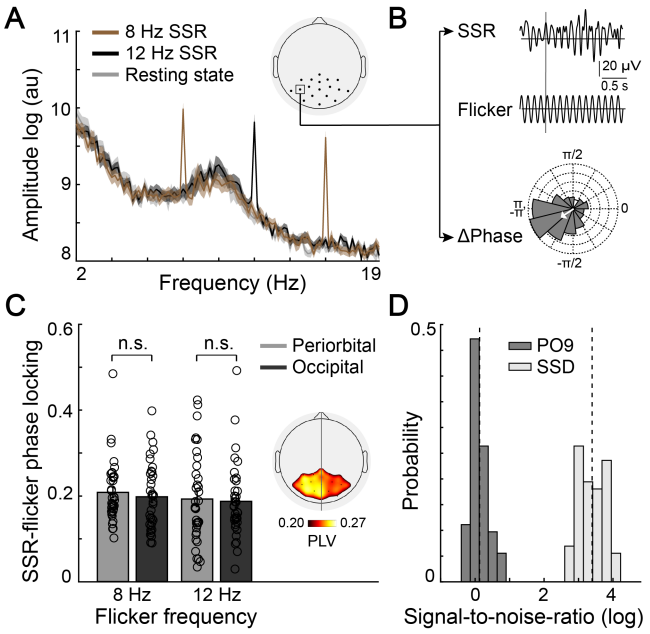

Fig 3. Sensory entrainment by visual flicker. (A) EEG amplitude spectra averaged across participants reveal peaks at the stimulation frequencies of 8 and 12 Hz (and the first harmonic at 16 Hz). Amplitude values were averaged across all recorded parieto-occipital electrodes. (B) Steady-state response (SSR) during 8 Hz flicker stimulation shown exemplary for one participant at electrode PO7. The absolute value of the mean time-dependent differences between SSR and flicker phase reveal the strength of phase alignment by visual flicker. (C) Phase alignment to flicker frequencies averaged across all electrodes did not differ between the occipital and periorbital tACS condition. Insert on the right shows the mean topography of EEG-flicker phase locking values (PLVs) averaged across both flicker frequencies, testing sessions and participants. Phase alignment is highest in visual areas of the left hemisphere contralateral to the flickering stimulus. (D) Reliable extraction of flicker-evoked 8 Hz activity by spatio-spectral decomposition (SSD). Compared to the best single channel, data obtained by SSD show larger signal-to-noise-ratios across all participants.

A basic prerequisite for phase-specific interference between visual and electric neuromodulation is the phase stability of flicker-evoked responses. We examined individual sensory entrainment by single visual flicker stimulation in the right lower visual field with spectral analysis of EEG data that was recorded prior to electrical stimulation. Amplitude spectra during visual stimulation showed peaks at the flicker stimulation frequencies and its harmonics (Fig 3A). To check for evoked neural phase stability, we computed the degree of SSR-flicker phase alignment for each participant (Fig 3B). Phase-locking values (PLVs) across all parieto-occipital electrodes were positively correlated between the two tACS conditions (8 Hz: $r = .61$, $p < .001$; 12 Hz: $r = .59$, $p < .001$). There was no significant difference in flicker phase entrainment across sessions (8 Hz: $t(35) = 0.93$, $p = .357$, $d_z = .16$; 12 Hz: $t(35) = 0.37$, $p = .716$, $d_z = .06$). Further, per testing session the strength of SSR-flicker phase locking was comparable between stimulation frequencies (periorbital: $t(35) = 0.85$, $p = .402$, $d_z = .14$; occipital: $t(35) = 0.69$, $p = .493$, $d_z = .12$). Topographies of PLVs reflect the spatial specificity of electrophysiological flicker responses, with maximum SSR-flicker phase alignment in the hemisphere contralateral to the flickering stimulus presented in the right visual field (insert in Fig 3C). Critically, to get

182 an optimal estimate of the tACS-targeted 8 Hz rhythm evoked by visual flicker, we applied
183 spatio-spectral decomposition (SSD) to data from all seven parieto-occipital electrodes
184 contralateral to the flicker [31]. SSD is a dimensionality reduction method that has been
185 repeatedly applied in the framework of flicker-evoked response analysis to optimally extract
186 rhythmic components in the data [32,33]. This procedure resulted in spatially weighted SSR_{SSD}
187 time series with larger signal-to-noise-ratio compared to single-channel analysis (Fig 3D).
188

189 Phase-dependent modulation of flicker brightness perception by 190 occipital tACS

191 To investigate whether the phase-shift between visual flicker and tACS modulated
192 perceived flicker brightness, we computed the proportion of brighter ratings of the LED_{8Hz}
193 relative to the LED_{12Hz} for each of the six LED_{8Hz}-tACS phase shift conditions. We quantified
194 the degree of tACS phase-dependence by a parametric alignment-based method. Herein, the
195 average brightness rating of the two bins adjacent to the bin opposite to the maximum brightness
196 rating bin (ADJ) is subtracted from the average rating of the two bins adjacent to the maximum
197 bin (MAX, Fig 4A) [34,35]. By excluding the maximum bin, analytical bias that might account
198 for phasic effects was prevented [35,36]. MAX-ADJ values greater than zero would reflect a
199 cyclic modulation of brightness ratings across flicker-tACS phase shifts. For the whole sample,
200 we did not observe a statistically significant modulation of perceived brightness by occipital or
201 periorbital tACS (periorbital: $t(35) = -0.41$, $p = .660$, $d_z = -.07$; occipital: $t(35) = 1.17$, $p = .125$,
202 $d_z = .19$) (Fig 4B left). Yet, as successful phase-specific interference of flicker and tACS is
203 expected to depend on stable flicker entrainment, we repeated the analysis after splitting the
204 sample in high and low flicker responders. Fig 4B shows tACS-induced brightness modulation
205 separately for the two subgroups sorted by mean 8 Hz SSR_{SSD}-flicker phase locking across both
206 tACS conditions. In accordance with our experimental rationale, participants with higher neural

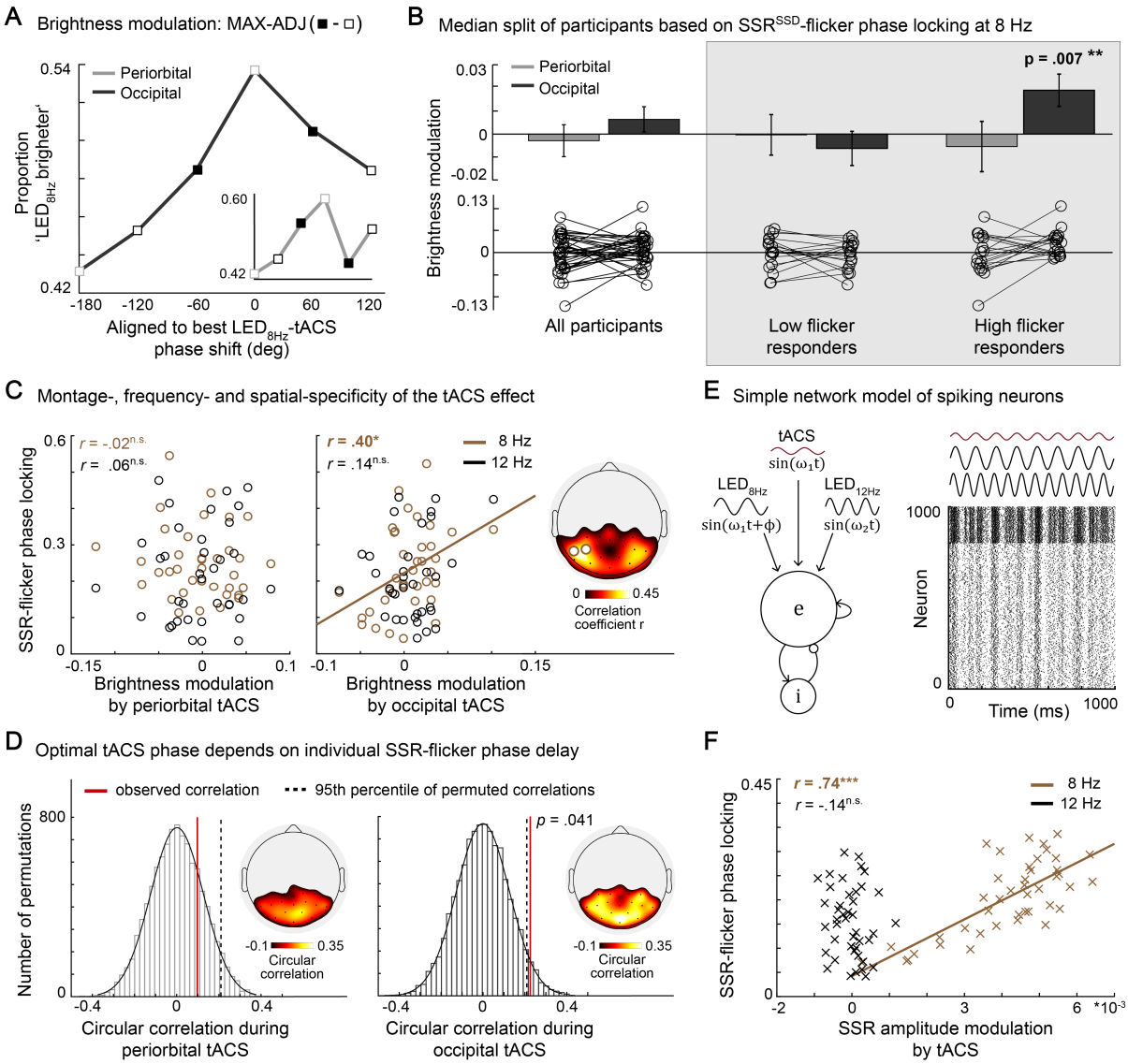

Fig 4. Phase-dependent modulation of flicker brightness perception by same-frequency tACS over the occipital cortex. (A) Proportion of brighter judgements of the LED_{8Hz} compared to LED_{12Hz} for one exemplary participant. The best LED_{8Hz}-tACS phase shift associated with highest brightness ratings is aligned to the center bin (0°). For statistical analysis, phase-dependent modulation was quantified by the MAX-ADJ measure as illustrated. (B) Across the whole sample, data show no significant phase-dependent modulation of brightness ratings for either tACS montage. Yet, after splitting participants based on their phase locking to the 8 Hz flicker, high flicker responders show a significant modulation of flicker brightness perception by occipital tACS. (C) Channel-level analysis shows a positive correlation between tACS effects on perception quantified by MAX-ADJ and phase locking of steady-state responses (SSR) to the 8 Hz flicker, exclusively under occipital tACS. Topography shows the spatial specificity of this correlation, localized to a significant electrode cluster in the visual cortex contralateral to the flickering stimulus. (D) The optimal flicker-tACS phase shift associated with greatest brightness judgements of the LED_{8Hz} is correlated with the individual phase delay between LED_{8Hz} onset and cortical SSR at 8 Hz. (E) Architecture of a simple model of spiking neurons, simulating the influence of concurrent tACS and flicker input on neuronal activity. Neuronal firing patterns are shown for 800 excitatory and 200 inhibitory neurons. (F) Simulations suggest a modulation of SSR amplitudes by phase-specific interference of visual and electric inputs and confirm behavioral results. Error bars represent the standard error. *p < .05, **p < .01, ***p < .001.

synchronization by the 8 Hz flicker showed a highly significant modulation of perceived brightness perception, exclusively under occiptal tACS (periorbital: $t(17) = -0.50$, $p = .688$, $d_z = -.12$; occipital: $t(17) = 2.71$, $p = .007$, $d_z = .64$). No brightness modulation by tACS was observed for participants showing only low SSR entrainment and, thus, less stable phase-locking to the 8 Hz flicker (periorbital: $t(17) = -0.04$, $p = .515$, $d_z = -.01$; occipital: $t(17) = -0.84$, $p = .794$, $d_z = -.20$).

tACS effect size on behavior depends on baseline oscillatory states

To further investigate the dependency of the tACS effect on flicker entrainment at the channel-level, we examined the correlation between the MAX-ADJ parameter and the SSR-flicker PLV per electrode, separately for each flicker frequency and tACS montage. Exclusively for the occipital tACS montage and the 8 Hz flicker, permutation statistics revealed a significant electrode cluster over the visual cortex (Fig 4C; cluster p-value: .012). Fig 4C shows the correlations between brightness modulation strength and SSR-flicker PLVs averaged across these cluster electrodes for both tACS montages and flicker frequencies ($\text{periorbital}_{8\ \text{Hz}}$: $r = -0.02$, $p = .914$; $\text{periorbital}_{12\ \text{Hz}}$: $r = 0.06$, $p = .731$; $\text{occipital}_{8\text{Hz}}$: $r = 0.40$, $p = .016$; $\text{occipital}_{12\text{Hz}}$: $r = 0.14$, $p = .401$). Importantly, the dependency of the tACS effects on SSR amplitudes was specific for the occipital stimulation montage, the tACS-modulated flicker frequency of 8 Hz and showed a spatially specific cluster-distribution contralateral to the visual flicker.

In order to gain mechanistic insight into the relation between perceptual modulation by tACS and flicker entrainment strength, we simulated the influence of sinusoidal electric and visual input in a simple network model of 1000 neurons based on Izhikevich [37]. While tACS input was given to all excitatory neurons, flicker input at 8 and 12 Hz was assigned to a logarithmically increasing percentage of excitatory neurons from 1 to 100 % to systematically simulate varying levels of flicker phase synchronization within the network. We simulated

neural spiking behavior under six different flicker-tACS phase shifts and computed resulting SSR amplitudes by averaging spectra across all excitatory neurons (Fig 4E). Converging with behavioral data, our network simulation replicates the observed positive relation between 8 Hz flicker entrainment strength and 8 Hz tACS effects, here quantified by the MAX-ADJ value of simulated SSR amplitudes (8 Hz: $r = 0.74$, $p < .001$; 12 Hz: $r = -0.14$, $p = .37$) (Fig 4F). Thus, network model simulations suggest a phase-specific neuronal interference between same-frequency flicker and tACS leading to systematic modulations of net SSR amplitudes.

Cortical phase delay of the SSR predicts the optimal timing of tACS application

While tACS is assumed to influence neuronal excitability with near zero phase lag, cortical SSRs show variable phase lags relative to flicker onset. Accordingly, the optimal tACS-flicker phase shift that enhances brightness perception is expected to vary across subjects. We computed the circular correlation between the optimal tACS phase and SSR-flicker phase delays at 8 Hz per electrode and tested for statistical significance by permutation statistics of the median correlation coefficient across all electrodes. As illustrated in Fig 4D, only for the occipital tACS montage, the SSR-flicker phase delay was predictive of the optimal tACS phase (median circular correlation $r = .22$, $p = .041$).

Discussion

In this multimodal study, we showed that biasing the temporal pattern of cortical excitability by tACS can influence the subjective brightness perception of upcoming rhythmic visual input. Critically, this phase-specific modulatory effect of tACS was only found when electrically stimulating the visual cortex, but not for the retinal control montage. The degree of

258 modulation depended on stable neural phase-locking to the targeted visual flicker and the delay
259 between visual presentation and cortical SSR. Converging with behavioral findings, neural
260 network simulations suggest an underlying amplitude modulation of neuronal steady-state
261 responses by tACS that depends on successful flicker-evoked phase stability. Together, our data
262 are best explained by cortical interference between flicker- and tACS-entrained rhythms. We
263 discuss this evidence in the context of a causal role of the amplitude of rhythmic brain activity
264 in the human visual cortex for brightness perception.

265 A major shortcoming in previous utilizations of tACS to examine cortical oscillations
266 was that most studies aimed to modulate brain activity with poor control over the underlying
267 phase of the targeted rhythm. While a number of studies investigated tACS effects on ongoing
268 or task-related neural activity in visual cortex [23,38–43], the low frequency- and phase-
269 consistency of the targeted rhythm can impede successful neural entrainment and, thus, hamper
270 rigorous investigations on behavioral implications of neuronal tACS effects. Here, we
271 combined visual and electrical rhythmic stimulation that enable the setting of the oscillatory
272 phase in the visual cortex and allow for an excellent control over the supposed tACS effect. In
273 this highly controlled stimulation paradigm, our data show that occipital tACS biases brightness
274 perception in a frequency- and phase-specific manner. As mean brightness ratings across
275 flicker-tACS phase shifts did not differ between occipital tACS and the periorbital tACS control
276 condition, data imply a phase-dependent enhancement and reduction of perceived brightness
277 under occipital electrical stimulation. This finding is in accordance with our previous study
278 results, demonstrating enlarged and suppressed SSR amplitudes depending on the flicker-tACS
279 phase shift [19]. Further, the fact that perceptual changes specifically depended on the strength
280 of neuronal phase locking to the tACS-targeted 8 Hz flicker, but not to the 12 Hz reference
281 flicker, favors an interference of entrained same-frequency rhythms. Thus, the clear relation
282 between tACS-flicker phase shift and brightness perception strongly points towards a
283 frequency- and phase-specific interference of neural activity in visual cortex that drives

284 behavioral changes.

285 The optimal timing of electrical neuromodulation relative to flicker onset leading to
286 highest brightness judgements showed pronounced interindividual variability. Crucially,
287 entrainment of the temporal pattern of neural activity by tACS is expected to facilitate or
288 hamper concurrent visual processing depending on their relative temporal alignment. While
289 tACS can instantaneously affect neural activity, SSRs typically show varying phase delays
290 relative to flicker onset, likely due to interindividual differences in SSR propagation along the
291 visual pathway and anatomical differences [44,45]. In the present data, circular correlation
292 analysis showed a predictive value of the cortical 8 Hz SSR phase delay for the optimal timing
293 of tACS application, exclusively for the occipital tACS montage. As the predictive value of the
294 cortical phase cannot be explained by an interaction between visual input and electric field in
295 the retina, the correlation additionally speaks against a mediation of occipital tACS effects on
296 SSR by retinal co-stimulation. Rather, these data are in support of a neuronal interference of
297 visually and electrically driven neuromodulation at a cortical level.

298 By interfering with cortical visual processing via tACS while keeping physical luminance
299 properties constant, our data corroborate potential mechanistic insight into the origin of
300 brightness coding. In the current literature, the link between neuronal response strength in the
301 visual cortex and brightness perception is, to our knowledge, exclusively correlative in nature
302 [2,4,10,46]. Proof for a causal role of the amplitude of SSRs for perception requires a
303 manipulation of neural activity independent of visual inputs. As electrophysiological recordings
304 during the application of tACS are contaminated by electrical artifacts, the direct measurement
305 of SSR amplitude changes by tACS is not feasible [47,48]. However, our simulations of
306 neuronal firing patterns to concurrent flicker and tACS input as well as our previous study
307 results [19] demonstrate that this SSR amplitude modulation is feasible, and that it depends on
308 stable entrainment of neural activity to the flicker. The behavioral data observed here reproduce
309 this relation between phase stability of tACS-targeted SSRs and resulting perceptual

310 modulations, suggesting a causal relation between the amplitude of rhythmic neural activity in
311 visual cortex and brightness perception. Due to limited focality of the tACS electric field, we
312 cannot exclude a role of higher-order top-down influence on perception. Yet, cluster analysis
313 located the predictive value of neuronal flicker-phase-locking for brightness perception at
314 electrodes positions PO7 and PO9 (according to the international 10-10 EEG system). Thus,
315 extending previous correlative results on the physiological substrate of brightness, we claim
316 that phase-specific neuronal interference of SSRs and electric field at first stages of visual
317 cortical processing causally translates into measurable perceptual changes.

318 For tACS applications, it is crucial to consider the role of potential peripheral stimulation
319 effects that might add to transcranial neuromodulation. Specifically, in case of visual perception
320 research, possible co-stimulation of the retinae due to current shunting across the scalp is a
321 potential caveat [26–28]. As even subthreshold and, thus, unconscious retinal stimulation might
322 lead to rhythmic entrainment along the visual pathway, exclusively relying on subjective
323 reports on phosphene perception might be an insufficient strategy [49,50]. Therefore, we used
324 an active tACS control montage explicitly tailored to induce subthreshold stimulation of the
325 retinae with individual adjustment of current intensities below phosphene threshold.
326 Simulations of electric fields demonstrated that estimated electric field strength in the eyes
327 under periorbital tACS (at 80 % phosphene threshold) was comparable to the expected current
328 density under occipital stimulation. As periorbital tACS had no modulatory influence on
329 brightness perception, data strongly suggest that the effect of occipital tACS on perception was
330 not mediated by subthreshold stimulation of the retinae.

331 In conclusion, we demonstrate that biasing sensory processing of flicker-evoked
332 responses by tACS influences the subjective experience of brightness in a frequency- and
333 phase-specific manner. This finding suggests a causal role of the amplitude of rhythmic brain
334 activity in visual cortex for brightness perception. Importantly, differences in tACS effects are
335 related to individual functional properties which emphasize the necessity for considering

336 potential sources of variability to approach custom-fit stimulation protocols. Transfer of the
337 advantageous methodological approach applied here to other sensory modalities may further
338 help to advance knowledge on the link between cortical sensory processing and perception.
339 Thus, by controlled modulations of brain signals, tACS can be utilized to deepen our
340 understanding of human brain function in basic and clinical science.

341

342

343 Materials and Methods

344 Participants

345 38 right-handed participants (mean age 25.74 ± standard deviation 4.06 years, 22 female,
346 16 male) volunteered for this study. All participants had normal or corrected-to-normal vision
347 and no history of psychiatric or neurological illness. Handedness was assessed via the short
348 version of the Edinburgh Handedness Inventory. Participants gave written informed consent
349 prior to participation and were monetarily compensated. The study was approved by the ethics
350 committee of the Hamburg Medical Association and conducted in accordance with the
351 declaration of Helsinki.

352

353 Experimental design

354 The experimental protocol was conducted on two separate days for occipital and
355 periorbital tACS. The order of tACS condition was counterbalanced across subjects. In the
356 beginning of each testing session, EEG was recorded in order to assess the physiological
357 response to visual flicker stimulation and the endogenous spectral properties of the brain during
358 resting-state. After psychophysical estimation of brightness discrimination thresholds for
359 individualization of physical luminance intensity, participants performed the main tACS

experiment. Participants were seated in an electromagnetically shielded, dimly lit room at a distance of 50 cm from the testing apparatus. Two light emitting diodes (LEDs) were placed at 3.4° visual angle in the lower visual field at 6.8° eccentricity from a central fixation dot and a polar angle of 45° from the horizontal meridian (Fig 1C). Diode LEDs had a diameter of 4 mm and were mounted in color mixing TIR lenses for sharp cut-off light distribution. Lenses were covered by light diffusion paper sheets, yielding a luminous surface with a diameter of 3 cm. The LEDs had a flicker frequency in the alpha band at 8 and 12 Hz. We assessed the nonlinear relation between forward voltage and luminance of each LED by a luminance meter (LS-100, Konica Minolta) and multiplied the resulting function with a pure 8 or 12 Hz sine to generate sinusoidal luminance signals.

Psychophysical estimation of brightness discrimination thresholds

Firstly, we determined the point of subjective equality between perceived brightness of the 8 and 12 Hz flicker. Based on previous studies showing interindividual differences in frequency-dependent brightness enhancement [29,30], the point of subjective equality was estimated individually for each participant by applying the method of limits [51]. During eight blocks, the LED_{8Hz} ascended from low to high intensity or descended from high to low intensity, relative to the LED_{12Hz}. The 12 Hz flicker was presented on the right side during the first four blocks and on the left side during the last four blocks. Single flicker trials had a duration of 2 sec and were followed by a 1 sec break. Blocks were interrupted by a 3 sec break. Participants responded per button press whenever they perceived brightness of the LED_{8Hz} matching brightness of the LED_{12Hz}. Within each block, variable starting and ending luminance intensities were used to avoid expectation errors [51]. The LED_{12Hz} was presented with constant peak luminance of 95 cd/m^2 (corresponding to 0.4 V peak-to-peak), while the 15 luminance intensities of the LED_{8Hz} ranged between 30 and 160 cd/m^2 (corresponding to 0.12 – 0.68 V peak-to-peak). Luminance was assessed by a luminance meter (LS-100, Konica Minolta). We

386 averaged the luminance intensities of the LED_{8Hz} selected by participants across 8 blocks to
387 determine the point of subjective equality between perceived brightness at the two flicker
388 frequencies.

389 Secondly, we estimated the psychometric function of the proportion of brighter
390 judgements of the LED_{8Hz} relative to the LED_{12Hz} depending on their luminance ratio. 12 evenly
391 distributed stimulus ratios, ranging from the priorly estimated point of subjective equality ± 0.5
392 V, were presented in random order by using the method of constants [51]. 20 trials each were
393 presented for the four highest and lowest stimulus intensities, and 30 trials for the intermediate
394 intensities (Fig 2A). Single flicker trials had a duration of 2 sec, followed by a break of 1.75 -
395 2 sec, comparable to the main tACS experiment. After each trial, participants indicated per
396 button press which of the two flickers appeared as brighter (or darker, depending on the
397 assigned condition that was counterbalanced across participants). We fit a logistic function to
398 each participant's data using a maximum likelihood criterion in the Palamedes toolbox [52].
399 Guess and lapse rate were fixed to .01 and the luminance ratios determined at [35, 42.5, 50,
400 57.5, 65] % brightness discrimination thresholds (Fig 2A).

401

402 **tACS experiment**

403 To test for tACS effects on conscious brightness perception, single flicker trials were
404 presented at luminance ratios around the individual brightness discrimination threshold. We
405 tested five luminance ratios between the two flickers at [35, 42.5, 50, 57.5, 65] % of the
406 discrimination threshold. tACS was continuously applied at 8 Hz. Single flicker trials started at
407 six different phases (0°, 60°, 120°, 180°, 240°, 300°) of the 8 Hz tACS cycle (Fig 1A). The
408 flicker phase angle at light onset of the LED_{8Hz} was set to 0°, while the LED_{12Hz} started
409 randomly at four different phase angles (0°, 90°, 180°, 270°). Single flicker trials had a duration
410 of 2 sec, followed by a break of 1.75 - 2 sec. After each trial, participants indicated the side of
411 flicker presentation appearing brighter per button press (or darker, depending on the assigned

412 counterbalanced condition). 19 trials were presented for each of the six tACS-LED$_{8Hz}$ phase
413 shift conditions and five flicker luminance ratios, resulting in 570 trials in total. Trial
414 presentation was subdivided in three blocks à 13.3 min, interrupted by 10 min breaks. Side of
415 flicker presentation and phase offsets were counterbalanced across tACS-LED$_{8Hz}$ phase shift
416 conditions.
417

418 # Transcranial electrical stimulation

419 During the tACS experiment, multi-electrode tACS was applied at 8 Hz via Ag/AgCl
420 electrodes (12 mm diameter) using neuroConn stimulators (DC-Stimulator plus, neuroConn,
421 Illmenau, Germany). One hour before tACS application, the skin beneath the stimulation
422 electrodes was prepared with EMLA cream for local anesthesia to reduce transcutaneous
423 stimulation effects by tACS (2.5 % lidocaine, 2.5 % prilocaine) (S1 Fig). Electrode impedances
424 were kept below 10 kΩ and comparable between electrodes to ensure an evenly distributed
425 electric field. During the tACS experiment of both sessions, stimulation was applied for 40 min
426 in total, divided in three blocks of 13.3 min duration including a linear ramp-up time of 6 sec
427 and another 6 sec at the final intensity before the start of visual stimulation.
428 For occipital tACS, current was applied via a 4 x 1 montage over the parieto-occipital
429 cortex at 4 mA peak-to-peak (Fig 1D). The stimulation montage was tailored to target the upper
430 bank of the calcarine sulcus, as described in detail below. A periorbital tACS montage served
431 as a control condition for sub-threshold stimulation effects of the retinae due to current shunting
432 across the scalp (Fig 1E). Current was applied via four electrodes placed superior and inferior
433 to the eyes with current flow in the vertical direction [53,54]. Stimulation intensities were
434 adjusted to 80% of the individual phosphene threshold [55]. Mean stimulation intensity was
435 0.071 ± 0.037 mA peak-to-peak. Peripheral tACS side-effects were systematically quantified
436 at the end of each session via a questionnaire, assessing the perceived strength and temporal
437 course of skin sensations, fatigue and phosphene perception (S1 Fig). Out of 38 participants,

438 two reported supra-threshold phosphene perception under occipital tACS and were therefore
439 excluded from data analysis.

440 For electric field simulation, a geometry-adapted hexahedral finite-element head model
441 was computed based on the ICBM-NY "New York Head" [56]. Point electrodes were simulated
442 [57] for the occipital and the periorbital tACS montages, respectively, and electric field
443 simulations were computed with the Simbio toolbox [58]. Electric field strength $|\vec{E}|$ was
444 quantified as the vector length at each location $\vec{x}$ of the electric field $\vec{E}$ as $\sqrt{[\vec{E}(\vec{x})]^2}$. Resulting
445 values in gray or white matter tissue were interpolated on the smoothed cortical surface of the
446 ICBM-NY using a spatial gaussian filter (5 mm width; Fig. 1D, left). Target electric field
447 strength $|\overrightarrow{E_t}|$ was computed as the average electric field strength in the putative stimulation
448 targets $\overrightarrow{x_t}$ in the left and right visual cortex (Fig 1D, right). Target locations $\overrightarrow{x_t}$ were defined
449 based on retinotopic maps of alpha oscillations evoked by visual stimuli in the lower quadrants
450 of the left and right visual field [22]. To estimate the electric field in the eyes, the surfaces of
451 the vitreous bodies of the eyes were extracted from the segmentation of cerebrospinal fluid
452 within the orbital cavity. Electric field strength $|\vec{E}|$ in cerebrospinal fluid was interpolated on
453 these surfaces using a spatial gaussian filter (5 mm width; Fig. 1E, left). Final electric field
454 strength $|\overrightarrow{E_{eye}}|$ was computed as the 0.95-percentile across all surface nodes of both vitreous
455 bodies and scaled to the individual intensities of the periorbital stimulation and to the common
456 intensity of the occipital stimulation montage (Fig 1E, right).

457

458 **Electrophysiological recording and data analysis**

459 EEG data were recorded from 18 Ag/AgCl electrodes (12mm diameter) mounted in
460 parieto-occipital regions in an elastic cap for 64 electrodes (Easycap, Herrsching, Germany).
461 We assessed 60 sec resting state EEG with eyes open and the electrophysiological response to

462 flicker stimulation while participants were presented with either 8 Hz or 12 Hz LED flickering
463 for 60 sec in the right lower visual field. Electrode impedances were kept below 20 kΩ. The
464 electrooculogram was recorded from two electrodes placed below the eyes. EEG signals were
465 referenced to the nose tip and recorded using BrainAmp MR plus amplifiers (Brain Products
466 GmbH, Gilching, Germany) and the corresponding software (Brain Products GmbH, Recorder
467 1.20). Data were recorded with an online passband of 0.016 - 250 Hz and digitized with a
468 sampling rate of 5 kHz.

469 EEG data were preprocessed and analyzed in Matlab (The MathWorks Inc.) using the
470 analysis toolbox FieldTrip [59] and custom-made scripts. Data were bandpass-filtered between
471 1 and 20 Hz using a Hamming-windowed sinc FIR (finite impulse response) filter (order 8250)
472 and segmented in 2 sec time epochs. We quantified the extent of visual entrainment by the
473 phase locking value (PLV) between EEG and visual flicker [60]. A Hilbert transform was
474 computed on the flicker and the EEG signal of each epoch and at each electrode. The time-
475 dependent differences of the flicker and EEG signal phase ($\phi_{flicker_t} - \phi_{EEG_t}$) for each
476 sample *t* served to compute the PLV

477 $$PLV = \left| \frac{1}{N_{epoch}} \sum_{k=1}^{N_{epoch}} \left(\frac{1}{N_{time}} \sum_{t=1}^{N_{time}} e^{i(\phi_{flicker_t} - \phi_{EEG_t})} \right) \right| \quad (1)$$

478 with N_{time} time steps per epoch, and N_{epoch} epochs. Comparability of flicker entrainment
479 strength between the two tACS sessions was computed by dependent samples t-tests for both
480 flicker frequencies.

481 To estimate the individual strength of flicker-evoked phase synchronization, we applied
482 spatio-spectral decomposition (SSD), a dimensionality-reduction method, to the EEG data.
483 SSD maximizes signal power at the frequency of interest while simultaneously minimizing
484 power at surrounding frequencies [31]. This procedure has been repeatedly applied in the
485 framework of flicker-evoked response analysis [32,33]. Based on PLV topography, we
486 computed SSD on all seven occipito-parietal electrodes contralateral to the flickering stimulus.

487 The signal covariance matrix was computed from bandpass filtered data around the flicker
488 frequency [$f_{flicker}$ – 0.25 Hz, $f_{flicker}$ + 0.25 Hz]. The noise covariance matrix was computed from
489 bandpass filtered data in the range of 2-19 Hz with a bandstop filter around the frequency of
490 interest at [$f_{flicker}$ – 1 Hz, $f_{flicker}$ + 1 Hz]. SSD was applied per participant and tACS condition
491 and the SSR_{SSD} component with the smallest eigenvalue was extracted for further analysis. To
492 quantify the gain in signal-to-noise-ratio by SSD, we segmented original data of each electrode
493 and SSR_{SSD} time series in 2 sec time epochs and computed the fast Fourier transform per epoch.
494 Signal-to-noise-ratio was defined as the ratio between the average amplitude at the stimulation
495 frequency and the mean amplitude at neighboring frequencies of [$f_{flicker}$ – 2 Hz, $f_{flicker}$ + 2 Hz].
496 Finally, we applied a Hilbert transform on the SSR_{SSD} signal and computed phase locking to
497 visual flicker (see Eq. 1).
498

499 # Statistical data analysis

500 To assess whether tACS modulates perceived flicker brightness in a phase-dependent
501 manner, we computed the proportion of brighter ratings of the LED_{8Hz} relative to the LED_{12Hz}
502 for each of the six LED_{8Hz}-tACS phase shift conditions. To quantify the degree of tACS phase-
503 dependence, we applied a parametric alignment-based method proposed by Riecke et al. [34]
504 and Zoefel at et. [35]. Herein, the maximum brightness rating condition was aligned to the
505 center bin and the remaining conditions were phase-wrapped. Then, the average brightness
506 rating of the two bins adjacent to the bin opposite to the center bin (ADJ) was subtracted from
507 the average brightness rating of the two bins adjacent to the center bin (MAX, Fig 4A). In case
508 of more than one optimal phase bin per participant, we repeatedly computed MAX-ADJ values
509 per optimal data bin alignment and conservatively took the average of MAX-ADJ values. By
510 excluding the center bin and the bin opposite to the center bin, analytical bias that might account
511 for reported tACS effects was prevented [35,36].

512 Statistical significance of brightness modulation across all participants was computed by
513 one-sample t-tests assessing whether MAX-ADJ values under occipital and periorbital tACS
514 were greater than zero. Effect sizes were determined by calculating Cohen's d_z. Further, as our
515 experimental rationale of phase-specific interference between flicker and tACS highly depends
516 on phase stability of flicker-evoked responses, we hypothesized a dependency of the tACS-
517 induced brightness modulation on individual flicker entrainment. Therefore, we split our
518 sample based on SSR_{SSD}-flicker phase locking and applied statistical significance testing of
519 brightness modulation for low and high flicker responders, respectively. To account for
520 multiple comparisons, significant test statistics are reported when the resulting *p*-values fell
521 below the Bonferroni-corrected alpha of $\alpha_{bonf} = .025$ (= .05/2).

522 To further investigate the frequency and montage specificity of tACS effects, we analyzed
523 the Pearson correlation between the strength of tACS modulation quantified by MAX-ADJ and
524 the degree of flicker entrainment as measured by SSR-flicker phase locking. For both flicker
525 frequencies and tACS conditions, Pearson correlation coefficients were computed at each
526 channel using cluster-based permutation tests to correct for multiple comparisons. Cluster-level
527 test statistics were calculated by taking the mean of correlation coefficients across neighboring
528 electrodes with significant correlations ($p < .05$) weighted by cluster size. The permutation
529 distribution was generated by between-subject randomization of PLVs across 10000 iterations.
530 We then averaged PLVs across significant electrode clusters and computed Pearson correlation
531 coefficients with MAX-ADJ values.

532 For investigating the predictability of the optimal timing of tACS application, we
533 computed the circular correlation coefficient between the individual SSR-flicker phase delay
534 and the optimal flicker-tACS phase shift leading to greatest brightness ratings. Therefore, we
535 fit one-cycle sine waves to brightness ratings and extracted the phase corresponding to the peak
536 of the sine. Statistical significance was tested by computing the permutation distribution of
537 median correlation coefficients across all electrodes between individual SSR phase delays and

randomly assigned optimal phase values across 10000 iterations. The observed circular correlation was considered statistically significant when exceeding the upper 5 % of the permuted distribution.

Neural network simulation

To validate our behavioral findings, we used a simple neural network model of spiking neurons and simulated the effect of visual and electric sinusoidal input on SSR amplitudes. The model was based on Izhikevich [37] and consisted of 1000 neurons [61] with random connections between excitatory (80 %) and inhibitory (20 %) neurons without plasticity of synapses. Each excitatory neuron was connected to 100 random neurons and each inhibitory neuron was connected to 100 excitatory neurons only. Synaptic conduction delays between 1 and 10 ms were assigned to excitatory connections and delays of 1 ms to inhibitory connections. Behavior of each neuron was simulated for 3 sec at a time step of 0.5 ms following the ordinary differential equations:

$$\frac{dv}{dt} = 0.04v^2 + 5v + 140 - u + I_{thal} + I_{tACS8} + I_{flicker8} + I_{flicker12} \quad (2)$$

$$\frac{du}{dt} = a * (0.2 * v - u) \quad (3)$$

if $v \geq 30\ mV$, then $v = -65, u = u + d$

with the neuronal membrane potential v and the membrane recovery variable u. The time scale and after-spike reset of the recovery variable were set to a = .04 and d = 8 for excitatory neurons and a = .2 and d = 2 for inhibitory neurons. Although the model is dimensionless, transmembrane voltage v and time t can be interpreted in units of mV and ms, respectively. I_{thal} represents the thalamic input to the neurons, with 10 random neurons receiving an input of 20 every millisecond. The network had mean firing rates of 11 Hz for excitatory and 41 Hz for inhibitory neurons. To simulate the influence of electrical and visual stimulation on neuronal

spiking behavior, the following three inputs were added:

$$I_{tACS8} = A_{tACS} * \sin(8\text{Hz} * 2\pi * t) \quad (4)$$

$$I_{flicker8} = A_{flicker8} * \sin(8\text{Hz} * 2\pi * t + \varphi_{flicker8_tACS8}) \quad (5)$$

$$I_{flicker12} = A_{flicker12} * \sin(12\text{Hz} * 2\pi * t + \varphi_{flicker12}) \quad (6)$$

with the amplitudes A and the phase shift φ between the flicker and tACS signal. I_{tACS8} was given to all excitatory neurons, while flicker input was assigned to a logarithmically increasing percentage of excitatory neurons from 1 to 100 % to systematically simulate varying levels of flicker phase synchronization within the network. We quantified the strength of flicker entrainment by simulating neural spiking behavior with A_{tACS}= 0 and computing the phase locking between the mean transmembrane voltage averaged across the last 2 sec of 800 excitatory neurons and the 8 Hz and 12 Hz flicker sine, respectively. Then, we added I_{tACS8} with a fixed amplitude ratio of 1:10 relative to the flicker inputs. The phase shift between I_{tACS8} and $I_{flicker8}$ was systematically varied (0°, 60°, 120°, 180°, 240°, 300°). $I_{flicker12}$ was started at one four randomly chosen phases relative to tACS (0°, 90°, 180°, 270°). To compute resulting SSR amplitudes, we demeaned voltage traces of the last 2 sec epoch per neuron and averaged spectra across all excitatory neurons. SSR amplitudes were defined as the ratio between the amplitude at the stimulation frequency and mean amplitude at the two neighboring frequencies. SSR amplitudes and phase locking values were averaged across 90 simulations. Modulation of SSR amplitudes dependent on the phase-shift between visual and electric inputs was then quantified by the MAX-ADJ measure.

Acknowledgements

We thank Karin Deazle and Rebecca Burke for assistance in data recording and Florian Pieper for methodological support.

Funding

This work was supported by the Deutsche Forschungsgemeinschaft (SFB 936/A3 awarded to A.K.E. and T.R.S.; SPP 1665/EN 533/13-1 and SFB TRR 169/B1 awarded to A.K.E.; SPP 1665/SCHN 1511/1-2 awarded to T.R.S.) and by the Studienstiftung des deutschen Volkes (awarded to M.F.).

References

1. Norcia AM, Appelbaum LG, Ales JM, Cottereau BR, Rossion B. The steady-state visual evoked potential in vision research: a review. J Vis. 2015;15: 4. doi:10.1167/15.6.4.doi

2. Rossi AF, Paradiso MA. Neural correlates of perceived brightness in the retina, lateral geniculate nucleus, and striate cortex. J Neurosci. 1999;19: 6145–6156. doi:10.1523/JNEUROSCI.19-14-06145.1999

3. Rossi AF, Rittenhouse CD, Paradiso MA. The representation of brightness in primary visual cortex. Science (80-). 1996;273: 1104–1107. doi:10.1126/science.273.5278.1104

4. Roe AW, Lu HD, Hung CP. Cortical processing of a brightness illusion. Proc Natl Acad Sci. 2005;102: 3869–3874. doi:10.1073/pnas.0500097102

5. MacEvoy SP, Paradiso MA. Lightness constancy in primary visual cortex. Proc Natl Acad Sci. 2001;98: 8827–8831. doi:10.1073/pnas.161280398

6. Duszyk A, Bierzyńska M, Radzikowska Z, Milanowski P, Kuś R, Suffczyński P, et al. Towards an optimization of stimulus parameters for brain-computer Interfaces based on steady state visual evoked potentials. Cymbalyuk G, editor. PLoS One. 2014;9: e112099. doi:10.1371/journal.pone.0112099

7. Regan D. Evoked potentials specific to spatial patterns of luminance and colour. Vision Res. 1973;13: 2381–2402. doi:10.1016/0042-6989(73)90237-X

8. Notbohm A, Kurths J, Herrmann CS. Modification of brain oscillations via rhythmic light stimulation provides evidence for entrainment but not for superposition of event-related responses. Front Hum Neurosci. 2016;10: 10.

615 doi:10.3389/fnhum.2016.00010

616 9. Andersen SK, Muller MM, Martinovic J. Bottom-up biases in feature-selective
617 attention. J Neurosci. 2012;32: 16953–16958. doi:10.1523/JNEUROSCI.1767-
618 12.2012

619 10. Boyaci H, Fang F, Murray SO, Kersten D. Responses to lightness variations in
620 early human visual cortex. Curr Biol. 2007;17: 989–993.
621 doi:10.1016/j.cub.2007.05.005

622 11. McCourt ME, Foxe JJ. Brightening prospects for "early" cortical coding of
623 perceived luminance. J Vis. 2010;3: 424–424. doi:10.1167/3.9.424

624 12. Pereverzeva M, Murray SO. Neural activity in human V1 correlates with
625 dynamic lightness induction. J Vis. 2008;8: 8–8. doi:10.1167/8.15.8

626 13. van de Ven V, Jans B, Goebel R, De Weerd P. Early human visual cortex
627 encodes surface brightness induced by dynamic context. J Cogn Neurosci.
628 2012;24: 367–377. doi:10.1162/jocn_a_00126

629 14. Thut G, Miniussi C, Gross J. The functional importance of rhythmic activity in
630 the brain. Curr Biol. 2012;22: R658–R663. doi:10.1016/j.cub.2012.06.061

631 15. Bergmann TO, Hartwigsen G. Inferring causality from noninvasive brain
632 stimulation in cognitive neuroscience. J Cogn Neurosci. 2021;33: 195–225.
633 doi:10.1162/jocn_a_01591

634 16. Krause MR, Vieira PG, Csorba BA, Pilly PK, Pack CC. Transcranial alternating
635 current stimulation entrains single-neuron activity in the primate brain. Proc
636 Natl Acad Sci. 2019;116: 5747–5755. doi:10.1073/pnas.1815958116

637 17. Vieira PG, Krause MR, Pack CC. tACS entrains neural activity while

638 somatosensory input is blocked. Hanslmayr S, editor. PLOS Biol. 2020;18:
639 e3000834. doi:10.1371/journal.pbio.3000834

640 18. Johnson L, Alekseichuk I, Krieg J, Doyle A, Yu Y, Vitek J, et al. Dose-
641 dependent effects of transcranial alternating current stimulation on spike timing
642 in awake nonhuman primates. Sci Adv. 2020;6: eaaz2747.
643 doi:10.1126/sciadv.aaz2747

644 19. Fiene M, Schwab BC, Misselhorn J, Herrmann CS, Schneider TR, Engel AK.
645 Phase-specific manipulation of rhythmic brain activity by transcranial
646 alternating current stimulation. Brain Stimul. 2020;13: 1254–1262.
647 doi:10.1016/j.brs.2020.06.008

648 20. Ruhnau P, Keitel C, Lithari C, Weisz N, Neuling T. Flicker-driven responses in
649 visual cortex change during matched-frequency transcranial alternating current
650 stimulation. Front Hum Neurosci. 2016;10: 184. doi:10.3389/fnhum.2016.00184

651 21. Chai Y, Sheng J, Bandettini PA, Gao J-H. Frequency-dependent tACS
652 modulation of BOLD signal during rhythmic visual stimulation. Hum Brain
653 Mapp. 2018;39: 2111–2120. doi:10.1002/hbm.23990

654 22. Popov T, Gips B, Kastner S, Jensen O. Spatial specificity of alpha oscillations in
655 the human visual system. Hum Brain Mapp. 2019;40: 4432–4440.
656 doi:10.1002/hbm.24712

657 23. Kasten FH, Duecker K, Maack MC, Meiser A, Herrmann CS. Integrating
658 electric field modeling and neuroimaging to explain inter-individual variability
659 of tACS effects. Nat Commun. 2019;10: 1–11. doi:10.1038/s41467-019-13417-
660 6

661 24. Opitz A, Falchier A, Yan C-G, Yeagle EM, Linn GS, Megevand P, et al.
662 Spatiotemporal structure of intracranial electric fields induced by transcranial
663 electric stimulation in humans and nonhuman primates. Sci Rep. 2016;6: 31236.
664 doi:10.1038/srep31236
665 25. Huang Y, Liu AA, Lafon B, Friedman D, Dayan M, Wang X, et al.
666 Measurements and models of electric fields in the in vivo human brain during
667 transcranial electric stimulation. Elife. 2017;6: 1–26. doi:10.7554/eLife.18834
668 26. Laakso I, Hirata A. Computational analysis shows why transcranial alternating
669 current stimulation induces retinal phosphenes. J Neural Eng. 2013;10: 046009.
670 doi:10.1088/1741-2560/10/4/046009
671 27. Kar K, Krekelberg B. Transcranial electrical stimulation over visual cortex
672 evokes phosphenes with a retinal origin. J Neurophysiol. 2012;108: 2173–2178.
673 doi:10.1152/jn.00505.2012
674 28. Schutter DJLG. Cutaneous retinal activation and neural entrainment in
675 transcranial alternating current stimulation: A systematic review. Neuroimage.
676 2016;140: 83–88. doi:10.1016/j.neuroimage.2015.09.067
677 29. Bertrand JK, Ouellette Zuk AA, Chapman CS. Clarifying frequency-dependent
678 brightness enhancement: delta- and theta-band flicker, not alpha-band flicker,
679 consistently seen as brightest. Exp Brain Res. 2019;237: 2061–2073.
680 doi:10.1007/s00221-019-05568-1
681 30. Bartley SH. Subjective brightness in relation to flash rate and the light-dark
682 ratio. J Exp Psychol. 1938;23: 313–319. doi:10.1037/h0054488
683 31. Nikulin V V., Nolte G, Curio G. A novel method for reliable and fast extraction

of neuronal EEG/MEG oscillations on the basis of spatio-spectral decomposition. Neuroimage. 2011;55: 1528–1535. doi:10.1016/j.neuroimage.2011.01.057

32. Tanaka H. Group task-related component analysis (gTRCA): a multivariate method for inter-trial reproducibility and inter-subject similarity maximization for EEG data analysis. Sci Rep. 2020;10: 84. doi:10.1038/s41598-019-56962-2

33. Bosse S, Acqualagna L, Samek W, Porbadnigk AK, Curio G, Blankertz B, et al. Assessing perceived image quality using steady-state visual evoked potentials and spatio-spectral decomposition. IEEE Trans Circuits Syst Video Technol. 2018;28: 1694–1706. doi:10.1109/TCSVT.2017.2694807

34. Riecke L, Formisano E, Sorger B, Başkent D, Gaudrain E. Neural entrainment to speech modulates speech intelligibility. Curr Biol. 2018;28: 161-169.e5. doi:10.1016/j.cub.2017.11.033

35. Zoefel B, Davis MH, Valente G, Riecke L. How to test for phasic modulation of neural and behavioural responses. Neuroimage. 2019;202: 116175. doi:10.1016/j.neuroimage.2019.116175

36. Asamoah B, Khatoun A, Mc Laughlin M. Analytical bias accounts for some of the reported effects of tACS on auditory perception. Brain Stimul. 2019. doi:10.1016/j.brs.2019.03.011

37. Izhikevich EM. Polychronization: computation with spikes. Neural Comput. 2006;18: 245–282. doi:10.1162/089976606775093882

38. de Graaf TA, Thomson A, Janssens SEW, van Bree S, ten Oever S, Sack AT. Does alpha phase modulate visual target detection? Three experiments with

tACS-phase-based stimulus presentation. Eur J Neurosci. 2020;51: 2299–2313. doi:10.1111/ejn.14677

39. Nakazono H, Ogata K, Takeda A, Yamada E, Kimura T, Tobimatsu S. Transcranial alternating current stimulation of α but not β frequency sharpens multiple visual functions. Brain Stimul. 2020;13: 343–352. doi:10.1016/j.brs.2019.10.022

40. Schwab BC, Misselhorn J, Engel AK. Modulation of large-scale cortical coupling by transcranial alternating current stimulation. Brain Stimul. 2019. doi:10.1016/j.brs.2019.04.013

41. Misselhorn J, Schwab BC, Schneider TR, Engel AK. Synchronization of sensory gamma oscillations promotes multisensory communication. eneuro. 2019;6: ENEURO.0101-19.2019. doi:10.1523/ENEURO.0101-19.2019

42. Kar K, Krekelberg B. Transcranial alternating current stimulation attenuates visual motion adaptation. J Neurosci. 2014;34: 7334–7340. doi:10.1523/JNEUROSCI.5248-13.2014

43. Herring JD, Esterer S, Marshall TR, Jensen O, Bergmann TO. Low-frequency alternating current stimulation rhythmically suppresses gamma-band oscillations and impairs perceptual performance. Neuroimage. 2019;184: 440–449. doi:10.1016/j.neuroimage.2018.09.047

44. Morgan ST, Hansen JC, Hillyard SA. Selective attention to stimulus location modulates the steady-state visual evoked potential. Proc Natl Acad Sci. 1996;93: 4770–4774. doi:10.1073/pnas.93.10.4770

45. Notbohm A, Herrmann CS. Flicker regularity is crucial for entrainment of alpha

730 oscillations. Front Hum Neurosci. 2016;10: 503. doi:10.3389/fnhum.2016.00503

731 46. Zhou H, Davidson M, Kok P, McCurdy LY, de Lange FP, Lau H, et al.
732 Spatiotemporal dynamics of brightness coding in human visual cortex revealed
733 by the temporal context effect. Neuroimage. 2020;205: 116277.
734 doi:10.1016/j.neuroimage.2019.116277

735 47. Noury N, Hipp JF, Siegel M. Physiological processes non-linearly affect
736 electrophysiological recordings during transcranial electric stimulation.
737 Neuroimage. 2016;140: 99–109. doi:10.1016/j.neuroimage.2016.03.065

738 48. Noury N, Siegel M. Phase properties of transcranial electrical stimulation
739 artifacts in electrophysiological recordings. Neuroimage. 2017;158: 406–416.
740 doi:10.1016/j.neuroimage.2017.07.010

741 49. Williams PE. Entrainment to video displays in primary visual cortex of macaque
742 and humans. J Neurosci. 2004;24: 8278–8288. doi:10.1523/JNEUROSCI.2716-
743 04.2004

744 50. Dehaene S, Changeux J-P. Experimental and theoretical approaches to
745 conscious processing. Neuron. 2011;70: 200–227.
746 doi:10.1016/j.neuron.2011.03.018

747 51. Kingdom FAA, Prins N. Psychophysics. Psychophysics: a practical
748 introduction: Second Edition. Elsevier; 2016. doi:10.1016/C2012-0-01278-1

749 52. Prins, N., Kingdom FAA. Palamedes: Matlab routines for analyzing
750 psychophysical data. http://www palamedestoolbox.org. 2009.

751 53. Gall C, Sgorzaly S, Schmidt S, Brandt S, Fedorov A, Sabel BA. Noninvasive
752 transorbital alternating current stimulation improves subjective visual

753 functioning and vision-related quality of life in optic neuropathy. Brain Stimul.
754 2011;4: 175–188. doi:10.1016/j.brs.2011.07.003

755 54. Haberbosch L, Datta A, Thomas C, Jooß A, Köhn A, Rönnefarth M, et al. Safety
756 aspects, tolerability and modeling of retinofugal alternating current stimulation.
757 Front Neurosci. 2019;13: 1–12. doi:10.3389/fnins.2019.00783

758 55. Khatoun A, Breukers J, Op de Beeck S, Nica IG, Aerts J-M, Seynaeve L, et al.
759 Using high-amplitude and focused transcranial alternating current stimulation to
760 entrain physiological tremor. Sci Rep. 2018;8: 8221. doi:10.1038/s41598-018-
761 26013-3

762 56. Huang Y, Parra LC, Haufe S. The New York Head—A precise standardized
763 volume conductor model for EEG source localization and tES targeting.
764 Neuroimage. 2016;140: 150–162. doi:10.1016/j.neuroimage.2015.12.019

765 57. Pursiainen S, Agsten B, Wagner S, Wolters CH. Advanced boundary electrode
766 modeling for tES and parallel tES/EEG. IEEE Trans Neural Syst Rehabil Eng.
767 2018;26: 37–44. doi:10.1109/TNSRE.2017.2748930

768 58. SimBio Development Group. SimBio: a generic environment for bio- numerical
769 simulations. Available from https//www.mrt.uni-jena.de/simbio.

770 59. Oostenveld R, Fries P, Maris E, Schoffelen J-M. FieldTrip: Open source
771 software for advanced analysis of MEG, EEG, and invasive electrophysiological
772 data. Comput Intell Neurosci. 2011;2011: 1–9. doi:10.1155/2011/156869

773 60. Lachaux J-P, Rodriguez E, Martinerie J, Varela FJ. Measuring phase synchrony
774 in brain signals. Hum Brain Mapp. 1999;8: 194–208. doi:10.1002/(SICI)1097-
775 0193(1999)8:4<194::AID-HBM4>3.0.CO;2-C

61. Izhikevich EM. Simple model of spiking neurons. IEEE Trans Neural Networks. 2003;14: 1569–1572. doi:10.1109/TNN.2003.820440

Supporting information

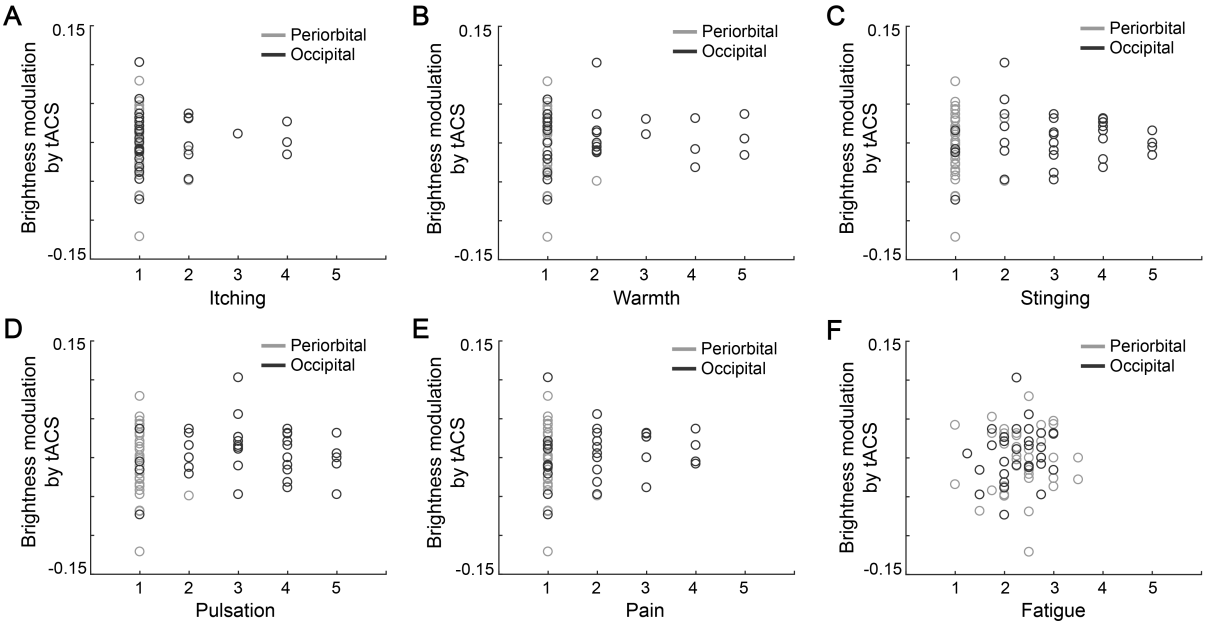

S1 Fig. Side effect characteristics during electrical stimulation. At the end of each testing session, participants rated the maximum perceived intensity of skin sensations (itching, warmth, stinging, pulsation), pain and fatigue on a five-point Likert scale. Fatigue values were averaged across four ratings during the course of each testing session. The relation between the strength of tACS-induced brightness modulation and side effects during periorbital and occipital tACS was tested by Pearson correlation coefficients. None of the correlation coefficients were statistically significant ($p > .05$).